Geo-climatic hazards in the eastern subtropical Andes: Distribution, Climate Drivers and Trends

Iván Vergara[1], Stella M. Moreiras[2, 3], Diego Araneo[2, 3] and René Garreaud[4, 5]

[1] CONICET-IPATEC, Bariloche, 8400, Argentina
[2] CONICET-IANIGLA, Mendoza, 5500, Argentina
[3] National University of Cuyo, Mendoza, 5502, Argentina
[4] University of Chile, Santiago, 8330015, Chile
[5] Center for Climate and Resilience Research, Santiago, 8320198, Chile

Correspondence to: Iván Vergara (ivergara@comahue-conicet.gob.ar)

Abstract. Detecting and understanding historical changes in the frequency of geo-climatic hazards (G-CHs) is crucial for the quantification of current hazards and project them into the future. Here we focus in the eastern subtropical Andes (32-33° S), using meteorological data and a century-long inventory of 553 G-CHs triggered by rainfall or snowfall. We first analyse their spatio-temporal distributions and the role of climate variability on the year-to-year changes in the number of days per season with G-CHs. Precipitation is positively correlated with the number of G-CHs across the region and year-round; mean temperature is negatively correlated with snowfall-driven hazards in the western (higher) half of the study region during winter and with rainfall-driven hazards in the eastern zone during summer. The trends of the G-CHs frequency since the mid-20th century were calculated taking cautions for their non-systematic monitoring. The G-CHs series for the different triggers, zones and seasons were generally stationary. Nonetheless, there is a small positive trend in rainfall-driven G-CHs in the eastern zone during summer congruent with a rainfall increase there. We also found a decrease in snowfall-driven G-CHs in the western zone since the late 1990's onwards, most likely due to a reduction in winter precipitation rather than to an increase in temperature.

1 Introduction

Geo-climatic hazards are natural phenomena that occur by a combination of atmospheric (e.g., precipitation, temperature, wind) and terrain factors (geotechnical and morphometric properties). This definition includes landslides, snow avalanches and phenomena of glacial (surges, GLOFs, IDLOFs) and fluvial origin (floods, lateral erosions, avulsions). All of them constitute an important risk along the Argentinean-Chilean Andes that runs for nearly 4000 km along the west part of South America, especially in its central portion (32-33° S) that has the highest erosion rates (Carretier et al., 2013), reaches more 5 km in elevation and where geo-climatic hazards have caused considerable human and economic losses mostly to the international traffic crossing this sector (e.g., Sepúlveda and Moreiras, 2013; Moreiras et al., 2018).

There is some work about historical and projected trends in the frequency of regional geo-climatic hazards (G-CHs; e.g., Moreiras, 2006; Moreiras and Vergara, 2017) but a quantitative analysis has not yet been carried out in order to attribute their origin. A first issue to elucidate is the origin of a seemingly increase in the number of G-CHs triggered by rainfall since the mid-20th century (Moreiras and Vergara, 2017), which could be due to an actual change in precipitation or to an increase in monitoring efforts during the last decades. A second question is on the origin of a decrease in the frequency of G-CHs triggered by snowfall since the end of the 1990s (Moreiras and Vergara, 2017). This could be due to a decrease in winter precipitation, an increase in the freezing level during these hazards due the ongoing regional warming or both (Masiokas et al., 2006; Vuille et al., 2015).

The purpose of this research is to assess the significance of the G-CHs trends and investigate their causes. To attribute these trends, we began by improving our general understanding of regional G-CHs analysing their distributions in time and space, and establishing their relationship with different climate elements. This research took advantage of a long, updated record of G-CHs in the eastern side of the subtropical Andes, with daily resolution and precise spatial location along a portion of an international, highly transited highway connecting Chile and Argentina. On the other hand, meteorological information is rather poor in this area, with few surface stations and absence of other measurement systems (radar, local radiosondes, etc.).

The paper is organized as follows. We begin by describing the physical characteristics of the area, the assembly of the G-CHs record and its usage. In the results section we present the spatio-temporal characterization of the G-CHs, followed by their association with the local climate and the temporary changes of the climatic variables and the G-CHs. In the discussion section, the results obtained are analysed, a future research direction is proposed, and a conceptual evaluation of the future geo-climatic hazard of the region is carried out. Finally, in the conclusions section, the most important results are described.

1.1 Study area and geographical setting

At subtropical latitudes (32-33° S) the Andes cordillera separates central Chile (to the west) and western central Argentina (to the east) with the border approximately following the highest peaks of the range, that reaches over 5 km ASL in this sector (Fig. 1). Here, an international road and the ex-Trasandino railway, links the cities of Los Andes (Chile) and Mendoza (Argentina). This is a major commercial and touristic route in use since the 17th century connecting the east and west side of the continent. G-CHs occur at both sides of the Andes (e.g., Sepúlveda and Moreiras, 2013; Sepúlveda et al., 2015) but here we focus on the eastern side because of the availability of a historical record taken in the Argentinean side of the road and railway, extending eastward from the border down to the plains near the city of Mendoza. This sector coincides with the middle and upper Mendoza river basin (Fig. 1a) and hosts more than 10 thousand inhabitants. Anthropic changes in the landscape are negligible due to the absence of significant cultivated areas and the limited infrastructure. The National Route 7 has currently an average traffic of about 3000 vehicles per day (ONDaT, 2018), maintained throughout the year due to domestic travels and the daily opening of the international pass, except when large snowfalls or major G-CHs occur.

The study area has elevations from 1250 to 5970 m ASL (when using a buffer of 15 km with respect to the Mendoza River that roughly encompassed all the terrain units studied; Fig. 1b). The lower limit of discontinuous permafrost is at 3700 m

ASL approximately (Trombotto et al., 1997). The area covered by perennial snow and glaciers (including inactive rock glaciers) is 103 km^2 (2.7 % of the total area; IANIGLA, 2018). The study area encompasses the morphotectonic units Cordillera Principal, Cordillera Frontal and Precordillera (Ramos, 1996), so the geotechnical, geological and morphometric characteristics vary widely. The first morphotectonic units are strongly altered by Quaternary glacial activity, with U-shaped valleys that have highly steep walls.

The vegetation types are Andean steppe and Monte scrubland (Paruelo et al., 2001) and their low density favours the triggering of landslides and snow avalanches. In the ravine headwaters there is a large amount of unconsolidated material generated by the seismic activity, the latest glaciations and the current cryoclasticism. Considering this factor and the dry climate of the region (described below), it is likely that the frequency and magnitude of debris flows are limited by the availability of water and not by debris supply. Debris flows are triggered by shallow failure planes and/or in-channel entrainment (Mergili et al., 2012) with little or no influence of the edaphic humidity generated by previous rainfall (Vergara et al., 2018). Jointed and partially weathered rock walls with slopes greater than 30° are prone to falls occurrence (Moreiras, 2005). Snow avalanches are usually triggered by snowfall (sudden overload), although they may be occur some weeks afterwards, due to earthquakes, rains or an increase in temperature and radiation.

Through photointerpretation and field surveys, Moreiras (2009) mapped a total of 869 landslides in the middle and upper Mendoza river basin. Based on that work, the abundance of the different types of landslides was established: debris flows 79%, falls 9%, rotational and translational slides 7%, and complex landslides 5%. More recently, Moreiras et al. (2012) used historical sources to describe 72 landslides and snow avalanches in the upper Mendoza river basin in the period 1822-2010, allowing an identification of their triggering causal factors (henceforth triggers or drivers): total precipitation 77%, snowmelt 14% and seismicity 9%. The most important conditioning factors of landslides in the middle Mendoza river basin are lithology and slope (Moreiras, 2005a).

1.2 Climate

The subtropical Andes, with its impressive altitude (>5000 m ASL), continuity and nearly north-south orientation, acts as a barrier separating two distinct climate regimes (Garreaud, 2009; Viale et al., 2019). The western side of the Andes receives most of the precipitation during austral winter (May-September) due to the arrival of cold fronts and other disturbances moving from the Pacific ocean (Falvey and Garreaud, 2007; Viale and Nuñez, 2011). In this side, frontal precipitation tends to be homogeneous (encompassing hundreds to thousands of kilometres) but tends to increase with altitude causing a vertical gradient in accumulation from about 300 mm yr^{-1} in the Chilean lowlands to about 1000 mm yr^{-1} atop of the Andes (e.g., Viale and Garreaud, 2015). The freezing level during winter storms is around 2500 m ASL (Garreaud, 2013) so that a significant portion of the precipitation over the western Andes is in the form of snow. Although the strong westerly flow atop of the Andes can spill over some snow towards its eastern side, the Argentinean sector receive most of the precipitation during austral summer (October to March; Viale and Garreaud, 2014) in connection with the southern edge of the South American Monsoon (e.g., Vera et al, 2006). In sharp contrast with the west side, precipitation to the east has a convective

nature and its water source is ultimately the Atlantic Ocean. These precipitation systems usually have an extension of 10 km^2 and intensities that can double those of the frontal systems (raw data of Vergara et al., 2018). The convection presents the maximum peak of probability during evening and early night, and minimum in the morning (Saluzzi, 1983).

100 In our study area (Fig. 1a), the western (wintertime frontal) and eastern (summertime convective) regimes have varying degrees of influences in the zonal direction (recall that the Andes axis is north-south oriented so moving in longitude the terrain altitude changes rapidly). Of course, there is a continuous change in the nature and seasonality of precipitation across the region (e.g., Fig. 2a) but a division into a western (W) an eastern (E) zones is useful for subsequent analyses. The mean elevation of W and E zones are 3740 and 2700 m ASL, respectively (Fig. 1b), and both have a similar zonal lengths

105 (between 43.6 and 46.1 km). The mean climate features were obtained by averaging the stations data available in each zone for the period 1993-2017 (Table 1). Because of the marked vertical gradients and the different features of valley sections where the stations are located, the monthly averages at each station were transformed into standardized anomalies before being averaged. The eastern (E), lower zone has a semi-arid climate with summer dominated, convective precipitation (Araneo et al., 2011; Fig. 2c). The climate of the western (W), higher zone is of the Tundra type (Sarricolea et al., 2016) with

110 frontal precipitation concentrated during austral winter (Fig. 2b-c). Note that both sectors share the same annual cycle of temperature, with warm summers and cold winters (Fig. 2d).

The regional precipitation has a high interannual standard deviation, about 35-40 % with respect to the annual average (Garreaud et al., 2009). El Niño Southern Oscillation (ENSO) is the major driver of these changes in the western sector / western side of the Andes, with a clear tendency for above (below) normal winter precipitation during El Niño (La Niña)

115 years (see review in Garreaud et al., 2009). Indeed, in the study area there is a positive correlation between the ENSO and the number of landslides and snow avalanches (Moreiras, 2005b, Moreiras et al., 2012). The Pacific Decadal Oscillation (PDO) and the Antarctic Oscillation (AAO) also modulate Andean precipitation. The PDO increase precipitation during its positive phases, while AAO does so during its negative phase (e.g., Masiokas et al., 2006). These oscillations have a greater impact on the wintertime precipitation. El Niño (La Niña) years also tend to produce above (below) normal precipitation in

120 the eastern half of our study region, although the ENSO impact on the monsoonal regime at subtropical latitudes is rather weak (e.g., Montecinos et al., 2000) and other large-scale modes also contribute to interannual variability in summer (e.g., Scian et al., 2005).

2 Data and methods

Our starting point for the present analysis is the historical record of landslides in the middle Mendoza river basin for the

125 period 1790-2003 (Moreiras, 2006) as well as the landslides and snow avalanches inventory in the upper Mendoza river basin for the period 1822-2010 (Moreiras et al., 2012). The recorded landslides and snow avalanches are concentrated in ravines, talus cones and rock walls adjacent to the valleys talwegs of the Mendoza and Uspallata rivers, where the routes and the railway are located. These terrain units were drawn with hydrological tools of the SAGA software (version 2.3.2) and

setting a minimum size of 0.2 km^2 for its individualization. The landslides and snow avalanches were assigned to the different terrain units either because the sources indicate the name of the activated ravine or the kilometre of the route or the railway that were cut. For the 18th and 19th centuries, the record is mainly composed by travellers' notes where the location and date of the hazards were usually indicated. For the 20th century, the record is mainly composed by articles from regional newspapers and written communications from railway and road companies. These sources indicate the date and position where the routes or the railway were blocked, and sometimes also inform the trigger, time and description of the main deposit. For the 21st century, field surveys of scientists from the Argentine Institute of Nivology and Glaciology were added, so the record became more detailed and the number of landslides and snow avalanches increased considerably. In addition to this, we continue using regional newspapers (El Andino, Los Andes Online, MDZ, Los Andes, Diario Uno, El Sol) as well as printed communications from Argentinean and Chilean customs and communications from road institutions (National Highway Management and Provincial Highway Management).

For each landslide and snow avalanche in the historical record, the most probable trigger was inferred from the original sources (the reports indicate if there were rain, snow, earthquakes, etc.) or were established using in-situ or satellite data. To decide on the occurrence of daily precipitation, we used 13 stations in the study area (Table 1) complemented by satellite estimates from the CMORPH daily product (Joyce et al., 2004; since 12/2002). The freezing level in the days with landslides and/or snow avalanches was estimated using daily mean temperature data at 8 surface stations (Table 1) from where the Zero Isotherm Altitude (ZIA) was calculated employing a wet adiabatic gradient of 6 °C km^{-1}. The freezing level was obtained subtracting 125 m from the ZIA to account the average distance that take for snow crystals to become liquid (Garreaud, 1992, White et al., 2010). Finally, to discard (or confirm) seismic-driven hazards we employed seismicity reports (USGS, 2018). In general, the most difficult trigger to identify was the rainfall during summer due to the reduced spatial extent of the convective systems that occur during this season. For rainfall-driven landslides identified during summer we first discard the action of an earthquake or a rapid melting of snow and/or ice (Vergara et al., 2020), and then confirm the occurrence of rain in some of the gauging stations and/or CMORPH.

In total, 683 landslides and snow avalanches were collected for the period 1790-2017. Snowfall and rainfall are the only triggers that we study here, therefore, 59 landslides triggered by earthquakes (9%), 16 landslides by rapid melting of snow and/or ice within the active layer (2%) and 55 landslides without an established trigger (8%) were excluded. In turn, of the 553 G-CHs triggered by rainfall or snowfall (Fig. 3), 35 were discarded because it was not possible to recover the precise geographic location. Since in many G-CHs the magnitude was not available we have refrained from using this variable. The record included the types of G-CHs: flow (31%; debris flow, mud flow, hyper-concentrated flow and debris avalanche), fall (33%; rock fall and debris fall) and snow avalanche (20%; Fig. 4). The remaining 16% corresponds to landslides where the type of movement could not be determined. The flow type was defined based on the characteristics of the G-CHs deposits, obviating the pre-failure mechanism. A priori, the percentages of this research and those calculated by Moreiras (2009; see Sect. 1.1) are not contradictory by the different methodology used. In particular, Moreiras (2009) mapped landslides regardless of their age and recurrence while here we limit the analysis to historical events.

Rainfall exclusively triggers landslides while snowfall can trigger snow avalanches and landslides. Indeed, about 35% of the snowfall-driven hazards in the W zone (high elevation sector) and the 83 % in the E zone (lower elevation sector) were rock or debris falls. During the snowfall these landslides can be triggered by short intervals of rain or by the melting of snow when it is deposited on the rock (and the consequent interstitial pressure in the fractures). The snow avalanches were considered to be triggered by snowfall, although they may be occur due to other causes (see Sect. 1.1). This simplification was done because the anomalous snowfall is the main atmospheric cause of its occurrence.

The greatest deficiency of the record is its generation from a non-systematic monitoring, depending on whether there was an observer that recorded a G-CH. To avoid to the maximum this error, most of the analyses were carried out for the period 1961-2017 (unless otherwise indicated). In 1961, the last section of international Route 7 was paved leading to a stabilization of traffic and G-CHs reports.

Using the G-CHs record, two time series were made. The first is the sum of all G-CHs during a given period (season or year) referred to as the *number of G-CHs*. The second is the sum, over a given period, of the number of days in which there was at least on G-CH, referred to as the *number of days*. The *number of G-CHs* is more representative of the spatial extent and intensity of the meteorological event but has a larger bias by non-systematic monitoring. We therefore use the *number of days* (with at least one G-CH) per season as our primary variable for analysis, segregating by trigger (snowfall, rainfall) and zone (W, E). In order to have a minimum number of cases in the segregated series that guarantees the robustness of the statistical analyses, we refrained here from making further subdivision based on terrain unit, G-CH type (landslide or snow avalanche) or landslide movement (flow or fall).

3 Results

3.1 Spatio-temporal distributions of G-CHs

Figure 5a show the probability of G-CHs annual occurrence for each ravine, talus cone and rock wall within our study region. As expected, snowfall-induced hazards are concentrated in the upper, western zone, although a few ones occur in the eastern, lower sector. Likewise, rainfall-induced landslides concentrate in the E zone but also extends into the W zone. The rainfall trigger has the 4 highest values (maximum probability 67 %) and the snowfall trigger the 5th and 8th highest values (maximum probability 40 %; Fig. 5a).

To obtain a more complete view of the G-CHs spatio-temporal distribution we calculated the monthly mean probability density of these hazards across the full study area (following the longitudinal axis) using the non-parametric kernel density estimator for directional-linear data (García-Portugués et al., 2013). The bandwidth was selected through the maximum likelihood cross-validation in order to optimize the trade-off between bias and variance (Hall et al., 1987). For this calculation, the day number of the year and the distance on the longitudinal axis of each G-CH were used. The methodology used allows considering the circular distribution of dates. The snowfall-driven hazards presented probability densities greater than the rainfall-driven landslides with a well-defined peak in W zone during May-June (early winter) but extending to the

full winter semester (Fig. 5b). The probability densities of the rainfall-driven hazards are more diffuse within the E zone and maximize at the height of the austral summer (Jan-Feb). Overall, the probability of G-CHs closely follows the annual cycle of the precipitation (Fig. 2a-c).

The snowfall-driven hazards are concentrated in the W because here the winter precipitation is greater and in solid state due to elevation. On the other hand, rainfall triggered landslides is greater in the E zone due to the lower elevation and the higher occurrence of intense, convective rainfall over this area during summer. While the snowfall trigger can only occur in the wintertime, due to the need for a low ZIA, the rainfall trigger can occur throughout the year, due to the fact that a sector of the E zone is below the mean freezing level of winter precipitation (Fig. 5a).

3.2 Association with climate drivers

We now establish the association between G-CHs with climate drivers (precipitation and temperature) at interannual time scales, considering the different combinations of seasons (winter, summer) and zones (W, E). An annual series of precipitation was calculated for each season and zone using the stations that have at least 89% of annual values of the 1982-2000 period. In total, three (four) stations of the W (E) zone were used. Each value of the series was expressed as a percentage of the common period, and then averages were calculated between the stations of the same zone. For the annual series of mean temperature, the available stations of each zone were used, that is to say: Punta de Vacas for the W zone and Uspallata and Guido for the E zone (Table 1). For the latter, simple averages were calculated as both records cover the same period.

Due to the non-normality in the precipitation and G-CHs series, the Spearman correlation coefficient was used. The significances of the correlations were evaluated with the method proposed by Zar (1972) considering a 95 % level of confidence (same percentage used in the following cases). Precipitation exhibits a positive correlation in all combinations, so that above (below) average precipitation tend to increase (decrease) G-CHs in both zones throughout the year (Fig. 6a). Winter precipitation is significantly correlated with snowfall-induced hazards across the whole study region, while summer precipitation is significantly correlated with rainfall-induced landslides in the East zone only (recall that summer rainfall in the West zone is low). The larger correlation values during winter in the W zone may results from the spatially coherent pattern of frontal precipitation, in contrast with the isolated, convective nature of summer precipitation. Another reason may be that the G-CHs of this spatio-temporal combination are generally snow avalanches which increase their occurrence probability with precipitation accumulation. On the contrary the falls and flows, most common in summer and E zone, depend on sub-daily precipitation intensity, data that is not available in this region.

Correlation values with average temperature are lower than those with precipitation and differ in sign among zones and seasons (Fig. 6b). The temperature is negatively and significant correlated with snowfall-driven hazards in the West zone during winter, and with rainfall-driven hazards in the East zone during summer. The weaker G-CHs–Temperature correlations may reflect the lack of a direct relationship between these variables, but rather an indirect association mediated

7

by precipitation (for instance, season with lower than average temperature may reflect a larger number of weather system crossing the region).

3.3 Contemporaneous changes

230   The linear trend over the period 1961 to 2017 for the precipitation and the G-CHs is calculated for each zone and season, using the non-parametric Mann-Kendall statistic (Mann, 1945, Kendall, 1975). The linear slope was estimated with the non-parametric statistic developed by Sen (1968). These methods are considered more adequate than least squares approach given the non-normality of the series. In the higher W zone, precipitation exhibit non-significant trends that differs between seasons: negative in winter (the wet season) and positive in summer (Table 2 and Fig. 7a,e). The winter drying trend is in

235   line with the negative rainfall tendency observed along the lowlands of central Chile (Boisier et al., 2016; 2018) that has been accentuated in the last decade in connection with the so-called central Chile mega drought (Garreaud et al., 2017; Rivera et al., 2017). Instead, in the E zone, precipitation has increased year round but only significantly during winter (Table 2 and Fig. 7b,f). These results coincide with the significant increase of precipitation in the central-western argentine plain that occurred mainly between December and May (SADSN, 2018; Labraga, 2010; Vera and Díaz, 2015). The trends in the E

240   and W zones remain similar when considering the full period 1957-2017 (Table 2).

Given their episodic nature, finding trends in the G-CHs frequency is more difficult. Nonetheless, rainfall-driven G-CHs show a significant increase in their number during summer over the E zone that is congruent with the weak precipitation increase in this sector and season (Fig. 7 b,d and Table 2).

The snowfall-driven winter hazards exhibit a decrease in the W zone since the end of the 1990s [-0.7 d with G-CHs decade^{-1}

245   for the 1997-2017 period (p<0.05); Fig. 7g]. This decrease may be connected with the precipitation decline or with an elevation of the freezing level due to the ongoing regional warming (Masiokas et al., 2006; Vuille et al., 2015). To assess the role of the temperature, we examine its evolution in the May-September season during the 1974-2017 period. To this end, we used surface temperature data from two nearby stations in the Chilean side (Lagunitas and Embalse el Yeso; Table 1). These stations were considered the most appropriate in terms of record length and data continuity, as well as elevation (>2400 m

250   ASL) and proximity to the study area (less than 80 km). For dry days we calculated the ZIA using a dry adiabatic gradient of 6.5 °C km^{-1} and for days with precipitation we calculated the freezing level (see Sect. 2).

The linear trends were calculated for the resulting ZIA series, through the least squares method. The ZIA for dry days has a significant trend of +4.31 m yr^{-1} (Fig. 8) in agreement with previous studies (Carrasco et al., 2008) and the overall warming over the subtropical Andes (Falvey and Garreaud, 2009; Vuille et al., 2015; Vergara et al., 2020). On the other hand, the

255   freezing level for days with precipitation had a very weak, non-significant trend of +0.42 m yr^{-1} (Fig. 8), similar to the trend obtained by Carrascto et al., (2005) in the annual ZIA for days with precipitation and notably lower than the trend during dry days. This suggest that the warming over the last decades has -for now- limited impact in the decrease in snowfall-driven G-CHs.

As an independent method, elevations of the main deposits of the snowfall-driven G-CHs for the periods 1882-1953 (39
cases) and 1993-2015 (52 cases) were compared (Fig. 9). The significance of difference in mean elevations between both
periods was determined through the non-parametric Bootstrap method (999 simulations; Zieffler et al., 2011). The mean
elevations of main deposits of the snowfall-driven G-CHs of both periods did not have a significant difference. These results
lend support to the notion that the decrease in snowfall-driven winter hazards is largely caused by the decline in Pacific-
sourced rainfall rather than an elevation in the ZIA due to regional warming.

4 Discussion

The seasonal mean temperature exhibits a weak and non-systematic correlation with the *number of days* with G-CHs,
reflecting the lack of a direct physical link between these variables. By contrast precipitation accumulated during winter is
positively associated with the *number of days* with snowfall-driven hazards in both zones, while summer rainfall is
correlated with the *number of days* with rainfall-driven landslides in the East zone. Although some of these correlations are
statistically significant, their values are not high enough to fit predictive models at interannual (Pavlova et al., 2014) or
meteorological event scale (e.g., Staley et al., 2017). An improved, denser meteorological network across this complex
terrain (including radar monitoring of summer convection) may result in a better depiction of the climate control of the local
geo-climatic hazard, suitable for a more quantitative diagnosis, forecast and projections of their future frequency.

Our trend analysis indicates that winter precipitation has been decreasing in the W zone. Although barely significant, this
decrease is associated with a more robust decline in frontal, Pacific-sourced precipitation in central Chile (Boisier et al.,
2016) and the occurrence of a decade-long drought in that region (Garreaud et al., 2017). On the other hand, we found an
overall increase in precipitation in the E zone. The trend is more significant in the winter semester due to the enhanced
moisture transport from the Atlantic to the east of the Andes (SADSN, 2018; Barros et al., 2014; Vera and Díaz, 2015). We
also studied the winter temperature given their control on altitude separating rainfall and snowfall (in close correspondence
with ZIA). In agreement with other evidence of regional warming, we found a clear increase in ZIA during dry days, which
are the majority in this region. In the subset of days with precipitation, however, the ZIA exhibits an insignificant increase,
suggesting that the thermal structure of winter, Pacific sourced storms hasn't changed enough yet to cause an impact on the
number of snowfall-driven G-CHs over the subtropical Andes.

Considering the interannual correlation between G-CHs and climate elements, as well as the tendencies of the later, we
advanced in the attribution of the trends in the *number of days* with snow avalanches and landslides. Finding trends in the G-
CHs frequency is complex given their highly variable nature and the non-systematic monitoring, resulting mostly in non-
significant values. Nonetheless, two series of G-CHs show significant trends. The first is the increasing *number of days* with
rainfall-driven hazards during summer over the E zone, in line with the weak precipitation increase in this sector and season.
Secondly, we confirm a decrease in the *number of days* with snowfall-driven hazards during winter in the W zone since the
end of the 1990s. We further show that such decrease is consistent with the decline in winter precipitation over central Chile

and the adjacent Andes, with little or no effect of the regional warming in the last decades since the freezing level during precipitating days exhibit an insignificant change.

When corrections for non-systematic monitoring are not applied (variable used, type and start year of trends) much larger tendencies are obtained. For example, when the trend of rainfall trigger, E zone and summer season G-CHs is calculated using *number of G-CHs* variable, the least squares method and the 1950-2017 period, a tendency of 1.5 G-CHs decade^{-1} is obtained, instead of 0.2 d with G-CHs decade^{-1} (consider that on average in a day with G-CHs there are 2.2 hazards; Figure 4b). This indicates that the previously found increase in the record of rainfall-driven G-CHs since the mid-20th century (Moreiras and Vergara, 2017) was mainly due to increases in monitoring.

A weakness of this study is to group processes with different nature such as falls and snow avalanches. This was done in order to have a minimum number of cases in the segregated series to perform statistical inferences, however, it generates some uncertainty about whether the results obtained are representative for all types of G-CHs grouped. Another weakness is that it does not account for the magnitude of landslides and snow avalanches. A future research direction, that may include this intensity metric, could be to stablish a relationship between the G-CHs and fluvial solid discharge, the latter showing to be a regionally good proxy of rainfalls (Garreaud and Viale, 2014). Positive results could add a magnitude proxy to the existing series and increase their reliability.

In closing this section, we speculate on the future prospect of geo-climatic activity over our study area. Model-based climate projections (e.g., Junquas et al., 2012; Vera and Díaz, 2015; Bozkurt et al., 2018) consistently reveal (a) a marked warming over the subtropical Andes, (b) a decline of Pacific-sourced, winter precipitation, and (c) an increase in Atlantic-sourced, monsoonal precipitation during the warm season. The last two projections, seemingly acting in the present, will result in the maintenance of the observed trends during the next decades: an increase in rain-driven hazards in the E zone and a decrease in snowfall-driven hazards in the W zone, eventually amplified by the projected warming.

5 Conclusions

In this work we have analysed a long record of G-CHs (including geo-location and possible trigger) in a sector extending from the subtropical Andean crest toward the lowlands of western Argentina (city of Mendoza) that follows a 90 km long transect of a highly used international highway. We focused our work on landslides and snow avalanches that can be triggered by rainfall and snowfall. The purpose of the research was to calculate the trends of the G-CHs and to explore their causes. The precautions taken before calculating trends were to separate spatially and temporally climate regimes and avoid as much as possible the effects of non-systematic monitoring. The G-CHs series for the different triggers, zones and seasons were generally stationary, however, two series had tendencies. The rainfall-driven G-CHs during summer over the E zone had an increase since the mid-20th century, which was related to the weak rainfall increase in that zone and season. The calculated increase is much lower than that which would have been obtained without corrections for non-systematic monitoring. On the other hand, snowfall-driven G-CHs in the W zone had a decrease since the late 1990's onwards. In this

case, non-systematic monitoring cannot explain the trend since it only increased over time. This change was attributed to a decrease in winter precipitation, since the snowline increase occurred mainly in days without precipitation.

325 **References**

AMC, Data of Lagunitas meteorological station, Data not available on the internet, 2018.

Araneo, D., Simonelli, S., Norte, F., Viale, M., and Santos, R.: Caracterización de sondeos estivales del norte de Mendoza mediante el análisis de componentes principales y obtención de un índice de convección, Meteorologica, 36(1), 31-47, 2011.

Barros, V. R., Boninsegna, J. A., Camilloni, I. A., Chidiak, M., Magrín, G. O., and Rusticucci, M.: Climate change in
330 Argentina: trends, projections, impacts and adaptation, WIREs Clim Change, 6, 151-169, 10.1002/wcc.316, 2015.

Boisier, J. P., Alvarez-garreton, C., Cordero, R. R., Damiani, A., Gallardo, L., Garreaud, R., Lambert, F., Ramallo, C., and Rojas, M.: Anthropogenic Drying in Central-Southern Chile Evidenced by Long-Term Observations and Climate Model Simulations, Elementa Science of the Antropocene, 6 (74), https://doi.org/10.1525/elementa.328, 2018.

Boisier, J. P., Rondanelli, R., Garreaud, R. D., and Muñoz, F.: Anthropogenic and natural contributions to the Southeast
335 Pacific precipitation decline and recent megadrought in central Chile, Geophys. Res. Lett., 43(1), 413-421, 2016.

Bozkurt, D., Rojas, M., and Boisier, J. P.: Projected Hydroclimate Changes over Andean Basins in Central Chile from Downscaled CMIP5 Models under the Low and High Emission Scenarios, Clim. Change, https://doi.org/10.1007/s10584-018-2246-7, 2018.

Carrasco, J. F., Casassa, G., and Quintana, J.: Changes of the 0°C isotherm and the equilibrium line altitude in central Chile
340 during the last quarter of the 20th century, Hydrol. Sci. J., 50(6), 933-948, 2005.

Carrasco, J. F., Osorio, R., and Casassa, G.: Secular trend of the equilibrium-line altitude on the western side of the southern Andes, derived from radiosonde and surface observations, J. Glaciol., 54(186), 538-550, 2008.

Carretier, S., Regard, V., Vassallo, R., Aguilar, G., Martinod, J., Riquelme, R., et al.: Slope and climate variability control of erosion in the Andes of central Chile, Geology, 41(2), 195-198, 2013.

345 DGA, Statistics of meteorological stations: www.dga.cl/, last access: 8 January 2018.

Falvey, M., and Garreaud, R.: Wintertime Precipitation Episodes in Central Chile: Associated Meteorological Conditions and Orographic Influences, J. Hydrometeorol., 8(2), 171-193, 2007.

Falvey. M., and Garreaud, R.: Regional cooling in a warming world: Recent temperature trends in the southeast Pacific and along the west coast of subtropical South America (1979-2006), J. Geophys. Res.: Atmos., 114(4), 1-16, 2009.

350 García-Portugués, E., Crujeiras, R. M., and González-manteiga, W.: Kernel density estimation for directional–linear data, J. Multivar. Anal., 121, 152-175, 2013.

Garreaud, R.: Estimación de la altura de la línea de nieve en cuencas de Chile central, Rev. Chilena de Ing. Hidráulica, 7, 21-32, 1992.

Garreaud, R.: Warm winter storms in Central Chile, J. Hydrometeor., 14, 1515-1534, 2013.

355 Garreaud, R., Alvarez-garreton, C., Barichivich, J., Boisier, J. P., and Christie, D.: The 2010 – 2015 megadrought in central Chile: impacts on regional hydroclimate and vegetation, Hydrol. Earth. Syst. Sci., 21, 6307-6327, 2017.

Garreaud, R., Viale, M.: Análisis de los fenómenos meteorológicos y climáticos que afectan la cuenca del río Maipo, Aquae Papers, 5(Special issue), 17-29, 2014.

Garreaud, R., Vuille, M., Compagnucci, R., and Marengo, J.: Present-day South American Climate, Palaeogeography,
360 Palaeoclimatology, Palaeoecology, 281(3-4), 180-195, 2009.

Hall, P., Watson, G. S., and Cabrera, J.: Kernel Density Estimation with Spherical Data, Biometrika, 74(4), 751-762, 1987.

IANIGLA-Inventario Nacional de Glaciares: http://www.glaciaresargentinos.gob.ar/, last access: 8 January 2018.

Joyce, R. J., Janowiak, J. E., Arkin, P. A., and Xie, P.: CMORPH: a method that produces global precipitation estimates from passive microwave and infrared data at high spatial and temporal resolution, J. Hydromet., 5, 487-503, 2004.

365 Junquas, C., Vera, C., Li, L., and Le Treut, H.: Summer Precipitation Variability over Southeastern South America in a Global Warming Scenario, Climate Dynamics, 38, 1867-1883, 2012.

Kendall, M. G. (Ed.): Rank correlation methods, Griffin, London, 1975.

Labraga, J. C.: Statistical Downscaling Estimation of Recent Rainfall Trends in the Eastern Slope of the Andes Mountain Range in Argentina, Theoretical and Applied Climatology, 99, 287-302, 2010.

370 Mann, H. B.: Non-parametric test against trend, Econometrica, 13, 245-259, 1945.

Masiokas, M. H., Villalba, R., Luckman, B. H., Le Quesne, C., and Aravena, J. C.: Snowpack Variations in the Central Andes of Argentina and Chile, 1951–2005: Large-Scale Atmospheric Influences and Implications for Water Resources in the Region, J. Clim., 19, 6334-6352, 2006.

Paruelo, J. M., Jobbagy, E. G., and Sala, O. E.: Current distribution of ecosystem functional types in temperate South
375 America, Ecosystems, 4, 683-698, 2001.

Mergili, M., Fellin, W., Moreiras, S. M., and Stötteret, J.: Simulation of debris flows in the Central Andes based on Open Source GIS: possibilities, limitations, and parameter sensitivity, Nat. Hazards, 61(3), 1051-1081, 2012.

Montecinos, A., Díaz, A., and Aceituno, P.: Seasonal Diagnostic and Predictability of Rainfall in Subtropical South America Based on Tropical Pacific SST, J. Clim., 13: 746-758, 2000.

380 Moreiras, S. M.: Climatic effect of ENSO associated with landslide occurrence in the Central Andes, Mendoza Province, Argentina, Landslides, 2(1), 53-59, 2005a.

Moreiras, S. M.: Landslide susceptibility zonation in the Rio Mendoza Valley, Argentina, Geomorphology, 66, 345-357, 2005b.

Moreiras, S. M.: Frequency of debris flows and rockfall along the Mendoza river valley (Central Andes), Argentina:
385 Associated risk and future scenario, Quat. Int., 158(1), 110-121, 2006.

Moreiras, S. M.: Análisis estadístico probabilístico de las variables que condicionan la inestabilidad de las laderas en los valles de los ríos Las Cuevas y Mendoza, Rev. Asoc. Geol. Argent., 65(4), 780-790, 2009.

Moreiras, S., Lisboa, M. S., and Mastrantonio, L.: The role of snow melting upon landslides in the central Argentinean Andes, Earth Surf Process Landforms, 37(10), 1106-1119, 2012.

390 Moreiras, S. M., and Vergara Dal Pont, I.: Climate Change Driving Greater Slope Instability in the Central Andes, in: Advancing Culture of Living with Landslides, edited by: Mikoš, M., Vilímek, V., Yin, Y., and Sassa, K., Springer, Cham, 191-197, 2017.

Moreiras, S. M., Vergara Dal Pont, I., and Araneo, D.: Were merely storm-landslides driven by the 2015-2016 Niño in the Mendoza River valley?, Landslides, 15(5), 997-1014, 2018.

395 ONDaT, Tránsito Medio Diario Anual (TMDA) en rutas nacionales: http://ondat.fra.utn.edu.ar/, last access: 8 January 2018.

Pavlova, I., Jomelli, V., Brunstein, D., Grancher, D., Martin, E., and Déqué, M.: Debris flow activity related to recent climate conditions in the French Alps: A regional investigation, Geomorphology, 219(4), 248-259, 2014.

Ramos, V. A.: Evolución tectónica de la Alta Cordillera de San Juan y Mendoza, in: Geología de la región del Aconcagua, provincias de San Juan y Mendoza, edited by: Ramos, V. A., et al., Dirección Nacional del Servicio Geológico, Buenos

400 Aires, 447-460, 1996.

Rivera, J., Penalba, O., Villalba, R., and Araneo, D.: Spatio-Temporal Patterns of the 2010–2015 Extreme Hydrological Drought across the Central Andes, Argentina, Water, 9(652), 2017.

SADSN, Cambio Climático en Argentina; Tendencias y Proyecciones: http://3cn.cima.fcen.uba.ar/3cn_informe.php, last access: 8 January 2018.

405 Saluzzi, M. E.: (1983) Aspectos físicos de la convección severa en Mendoza. PhD Thesis, Universidad de Buenos Aires, ARG.

Sarricolea, P., Herrera-Ossandon, M., and Meseguer-Ruiz, Ó.: Climatic regionalisation of continental Chile, J. Maps., 13(2), 66-73, 2016.

Scian, B., Labraga, J. C., Reimers, W., and Frumento, O.: Characteristics of Large-Scale Atmospheric Circulation Related to

410 Extreme Monthly Rainfall Anomalies in the Pampa Region, Argentina, under Non-ENSO Conditions, Theoretical and Applied Climatology, 85, 89-106, 2006.

Sen, P. K.: Estimates of the regression coefficient based on Kendall's tau, J. Am. Statist. Assoc., 63, 1379-1389, 1968.

Sepúlveda, S. A., Moreiras, S. M., Lara, M., and Alfaro, A.: Debris flows in the Andean ranges of central Chile and Argentina triggered by 2013 summer storms: characteristics and consequences, Landslides, 12(1), 115-133, 2015.

415 Sepúlveda, S. A., and Moreiras, S. M.: Large volume Landslides in the Central Andes of Chile and Argentina (32º-34ºS) and related hazards, Bulletin of Engineering Geology and the Environment, 6, 287-294, 2013.

SMN, Meteorological stations network: https://back.argentina.gob.ar/interior, last access: 8 January 2018.

Staley, D., Negri, J., Kean, J., Laber, J., Tillery, A., and Youberg, A.: Prediction of spatially explicit rainfall intensity-duration thresholds for post-fire debris-flow generation in the western United States, Geomorphology, 278, 149-162, 2017.

420 Trombotto D., Buk, E., and Hernández, J.: Monitoring of Mountain Permafrost in the Central Andes, Cordon del Plata, Mendoza, Argentina, Permafrost. Periglac., 8(1), 123-129, 1997.

USGS, Earthquake Catalog: www.earthquake.usgs.gov/earthquakes/search/, last access: 8 January 2018.

Vera, C., and Díaz, L.: Anthropogenic Influence on Summer Precipitation Trends over South America in CMIP5 Models, Int. J. Climatol., 35, 3172-3177, 2015.

Vera, C., Higgins, W., Amador, J., Ambrizzi, T., Garreaud, R., Gochis, D., Gutzler, D., et al.: Toward a Unified View of the American Monsoon Systems, J. Clim., 19, 4977-5000, 2006.

Vergara Dal Pont, I., Moreiras, S.M., Santibañez, F., Araneo, D., and Ferrando, F.: Debris flows triggered from melt of seasonal snow and ice within the active layer in the Semi-Arid Andes, Permafrost. Periglac., 31(1), 57-68, 2020.

Vergara Dal Pont, I.P., Santibañez, F., Araneo, D., Ferrando, F., and Moreiras, S.: Determination of probabilities for the generation of high-discharge flows in the middle basin of Elqui River, Chile, Nat. Hazards., 93(1), 531-546, 2018.

Viale, M., Bianchi, E., Cara, L., Ruiz, L., Villalba, R., Pitte, P., Masiokas, M., Rivera, J., and Zalazar, L.: Contrasting Climates at Both Sides of the Andes in Argentina and Chile, Frontiers in Environmental Science, 7(69), 10.3389/fenvs.2019.00069, 2019.

Viale, M., and Garreaud, R.: Summer Precipitation Events over the Western Slope of the Subtropical Andes, Monthly Weather Review, 142, 1074-1092, 2014.

Viale, M., and Garreaud, R.: Orographic effects of the subtropical and extratropical Andes on upwind precipitating clouds, J. Geophys. Res.: Atmos., 120(10), 4962-4974, 2015.

Viale. M, and Nuñez, M.: Climatology of Winter Orographic Precipitation over the Subtropical Central Andes and associated synoptic and regional characteristics, J. Hydrometeor., 12, 481-507, 2011.

Vuille, M., Franquist, E., Garreaud, R., Sven, W., Casimiro, L., and Cáceres, B.: Impact of the global warming hiatus on Andean temperature, J. Geophys. Res.: Atmos., 120(9), 3745-3757, 2015.

White, A. B., Gottas, D. J., Henkel, A. F., Neiman, P. J., Ralph, F. M., and Gutman, S. I.: Developing a performance measure for snow-level forecasts. J. Hydrometeor., 11,739-753, 2010.

Zar, J.: Significance Testing of the Spearman Rank Correlation Coefficient. J. Am. Statist. Assoc., 67(339), 578-580, 1972.

Zieffler, A. S., Harring, J. R., and Long, J. D.: Comparing Groups: Randomization and Bootstrap Methods Using R, Wiley, New York, 2011.

Table 1: Stations used and their main characteristics. The registration period does not consider interruptions. The stations without asterisks were used for triggers determination and statistical analysis, and those with one (two) asterisks only for triggers determination (statistical analysis).

Station	Institution	Elevation (m ASL)	Coordinates (° S and W)	Record (yr) Precipitation	Record (yr) Temperature
West zone					
Riecillos	DGA	1290	32.92-70.36	1929-	-
Lagunitas**	AMC	2765	33.07-70.26	1959-2014	1974-2014
Embalse el Yeso**	DGA	2475	33.68-70.09	1962-	1962-
Cristo Redentor*	SMN	3829	32.83 70.06	1965-1984	1956-1985
Horcones*	SMN	2988	32.81-69.94	1955-	1999-
Puente del Inca*	SMN	2733	32.82-69.90	1956-1976	1956-1976
Punta de Vacas	SMN	2441	32.88-69.77	1992-	1992-
Punta de Vacas II*	SMN	2405	32.85-69.76	1998-2007	1998-2007
Polvaredas	SMN	2249	32.79-69.65	1983-	-
East I zone					
San Alberto	SMN	2190	32.47-69.41	1983-	-
Uspallata II	SMN	1885	32.60-69.35	1962-2014	1962-2014
Uspallata	SMN	1896	32.59-69.34	1983-	1993-
East II zone					
Guido	SMN	1418	32.92-69.24	1957-	1965-
Potrerillos	SMN	1448	32.96-69.20	1983-	-
Cacheuta**	SMN	1270	33.01-69.12	1983-	-
Cerro Pelado*	SMN	3047	32.76-69.10	1983-	-

Table 2: Decadal changes in the precipitation percentage (Pp), the *number of days* with snowfall-driven G-CHs (S) and the *number of days* with rainfall-driven G-CHs (R). The values with asterisks are significant at 95 %, the empty spaces correspond to data not available.

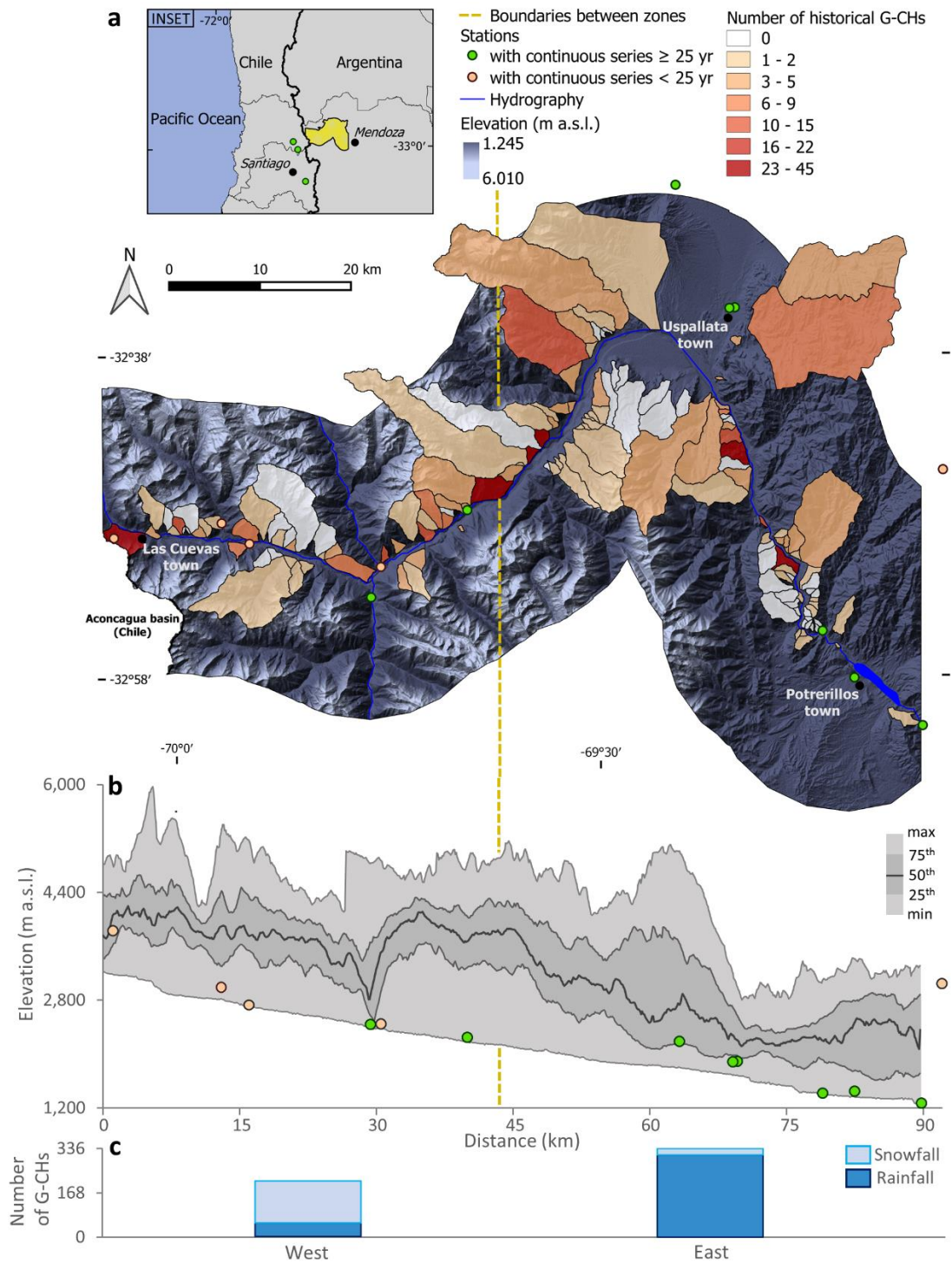|	1957-2017 Summertime			1957-2017 Wintertime			1961-2017 Summertime			1961-2017 Wintertime		
	Pp	S	R	Pp	S	R	Pp	S	R	Pp	S	R
West	1.07			-1.07			0.90		0.00	-3.91	0.00	0.00
East	5.12			6.70*			4.53		0.20*	8.46*	0.00	0.00

Figure 1: Main features of the study area and G-CHs. (a) Location of the study area (inset) and number of G-CHs for each ravine, talus cone and rock wall monitored superimposed on a topographic map. **(b)** Topographic profile along the Mendoza river. **(c)** G-CHs number for each trigger and zone. The yellow line in panels (a) and (b) delimits zones W and E.
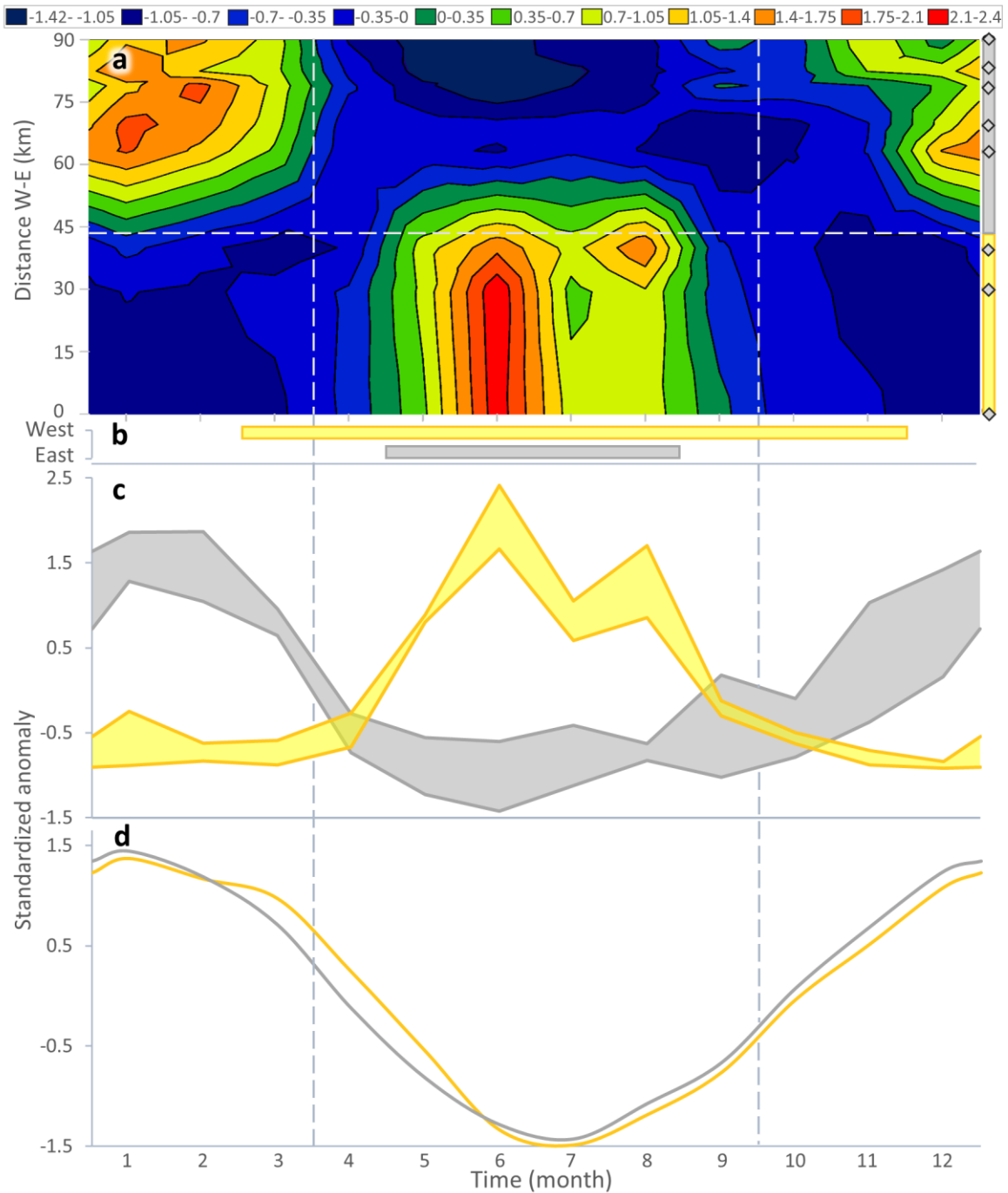
Figure 2: Mean annual cycles of selected variables. (a) Monthly mean standardized precipitation along a west-east transect. The vertical axis indicates the distance eastward from the Andes ridge. Diamonds indicate the stations positions, vertical lines the seasonal division and horizontal line the longitudinal division. (b) Periods of prevailing precipitation by frontal systems in each zone. (c) Range of monthly mean standardized precipitation considering the stations in each zone. (d) Mean average standardized temperature in each zone. In panels (b), (c) and (d) yellow (grey) lines refers to the W (E) zone.

480

485

490

495
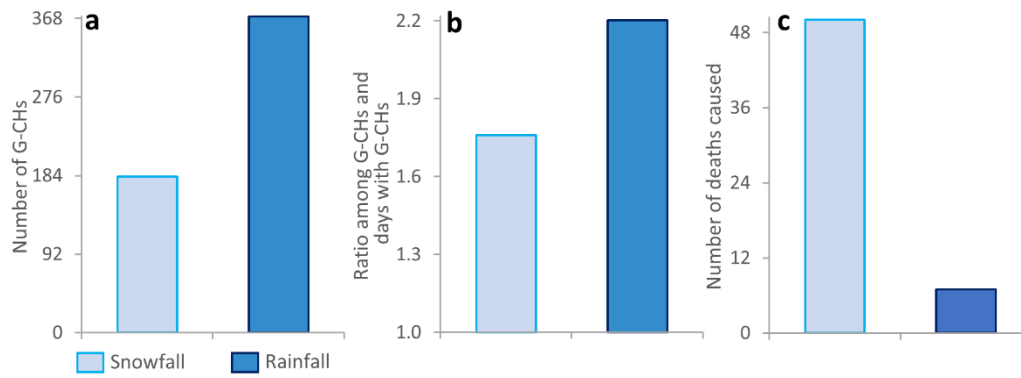
Figure 3: Main statistics of the G-CHs triggers considering the entire record. (a) Total number, (b) relationship between *number of G-CHs* and *number of days* with G-CHs, (c) associated fatalities.

Figure 4: Pictures illustrating G-CHs in study area: (a,c) rainfall-driven debris flow occurred on 2 February 2016 in the E zone, (b,d) rainfall-driven debris flow occurred on 23 January 2016 in the E zone, (e) rainfall-driven debris flow occurred on 4 February 2018 in the E zone, (f) rainfall-driven debris falls occurred on 2 August 2013 in the E zone, (g,h) snow avalanches in the W zone.
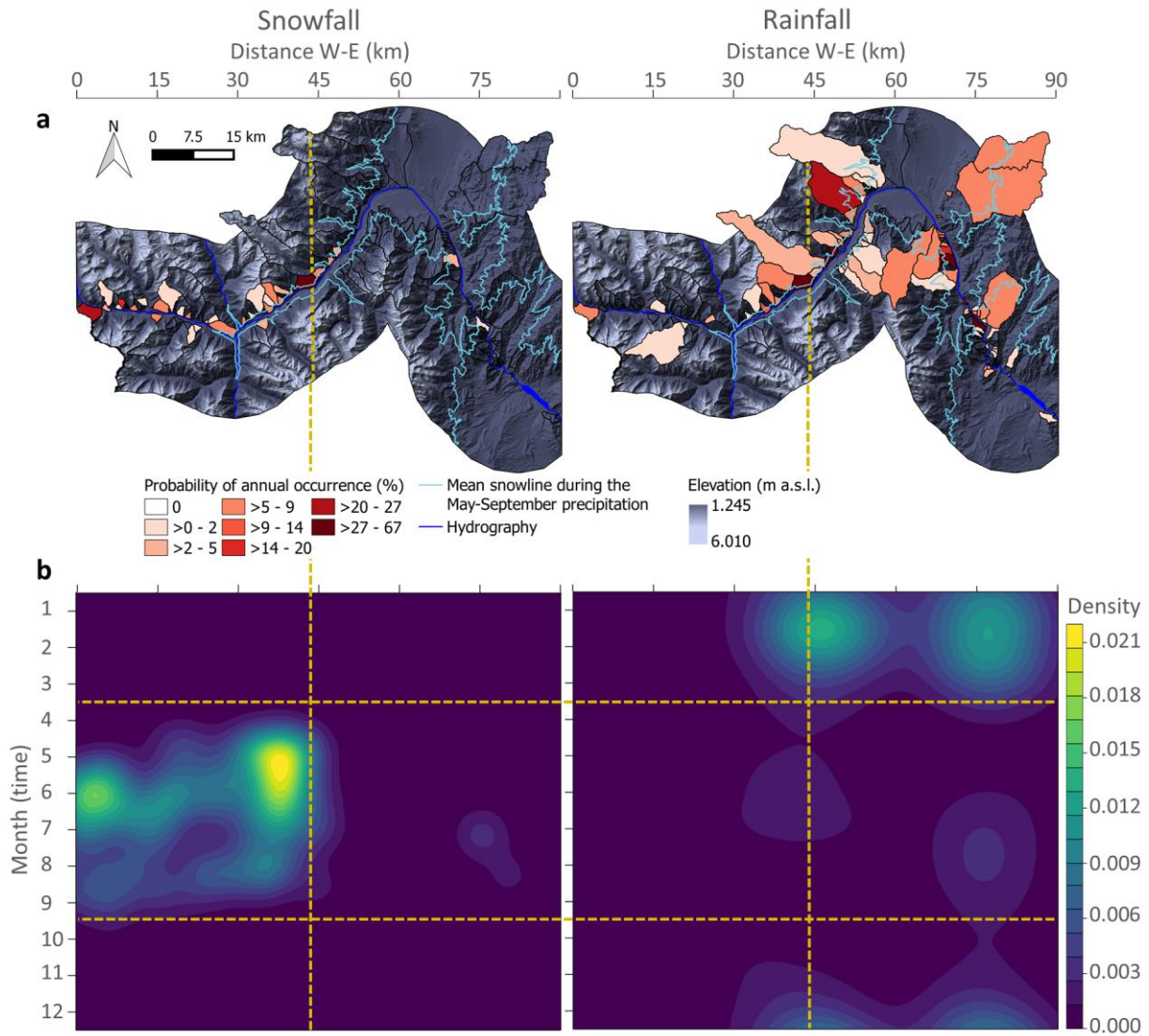
Figure 5: Distributions of the two triggers of G-CHs. (a) Probability of G-CHs annual occurrence for each ravine, talus cone and rock wall monitored superimposed on a topographic map. (b) Monthly mean probability density along a west-east transect for snowfall (left panel) and rainfall (right panel). The horizontal axis indicates the distance eastward from the Andes ridge. The cyan lines indicate the mean winter freezing level. Horizontal lines indicate the seasonal division and vertical line the longitudinal division.
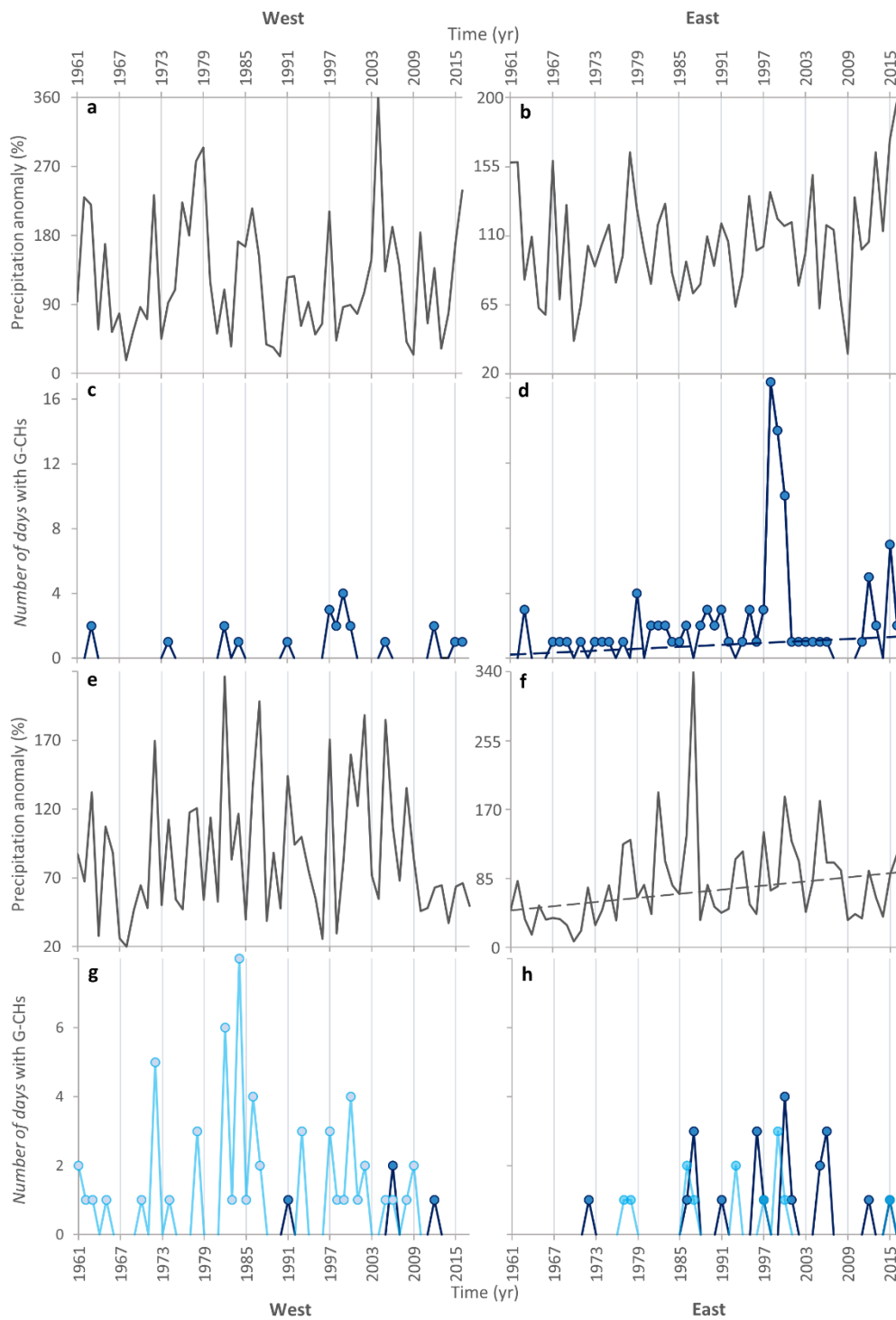
505

510
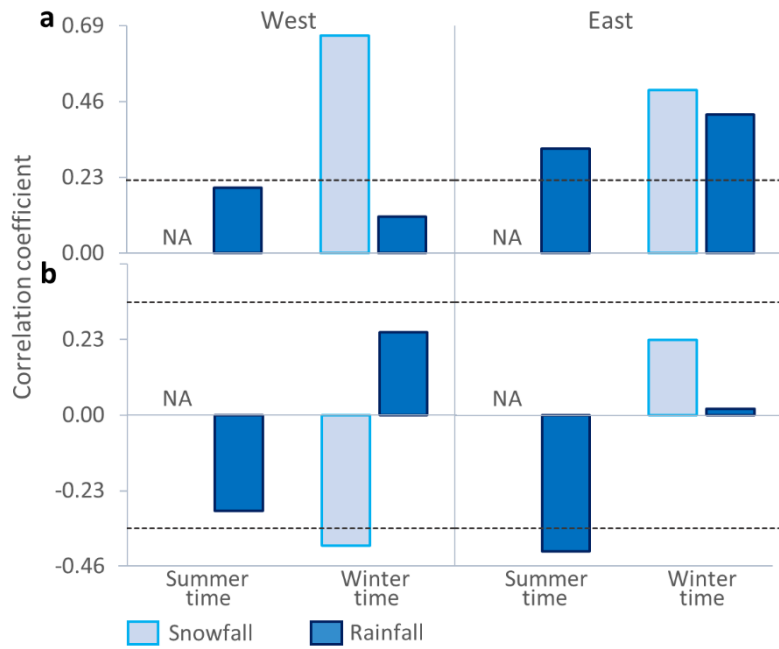
Figure 6: Interannual correlations between the series of the *number of days* with G-CHs per season and: (a) precipitation and (b) mean temperature. Dashed lines indicate significance at 95 % level.

525

Figure 7: Trends in drivers and G-CHs. Series of precipitation (grey lines) and *number of days* **with G-CHs (lines with points) in the W zone (left column) and E zone (right column) for: (a-d) summer and (e-h) winter months. In the case of G-CHs, blue colour refers to rainfall-driven hazards and light-blue to snowfall-driven hazards. Dashed lines indicate significant trends at 95 % level.**

22
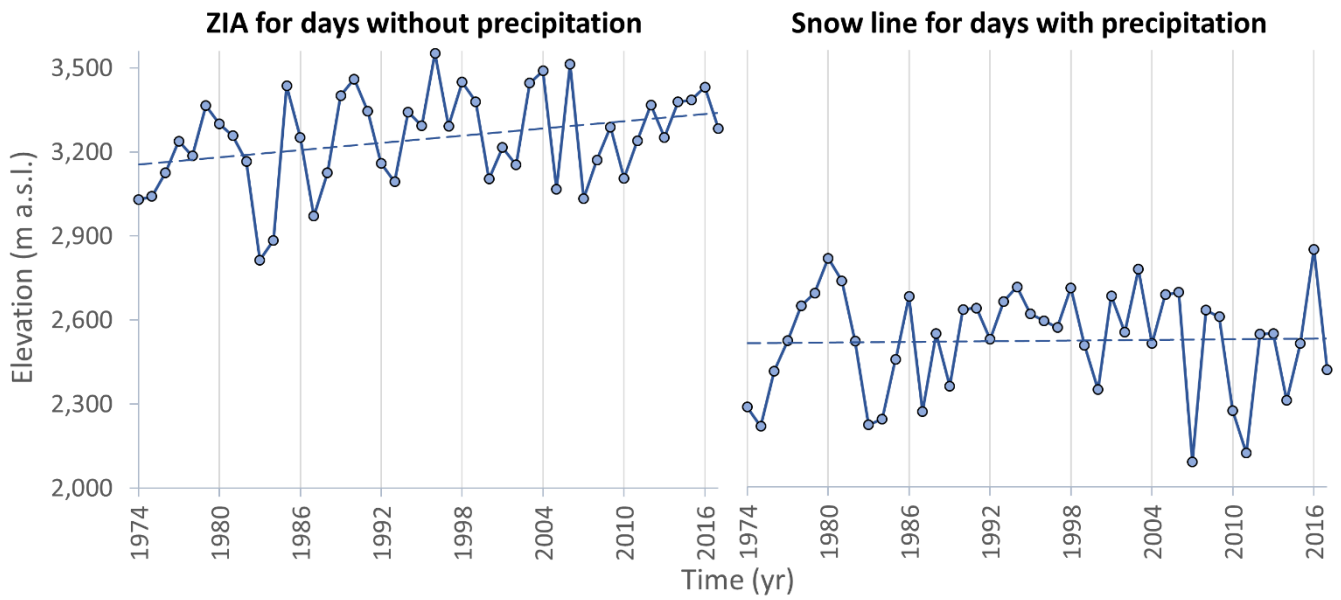
530   Figure 8: Warming effects. Left panel: annual series for the May-September average of the Zero-degree isotherm altitude during
dry days. Right panel: annual series for the May-September average of the snowline during days with precipitation. Dashed lines
indicate the trends.
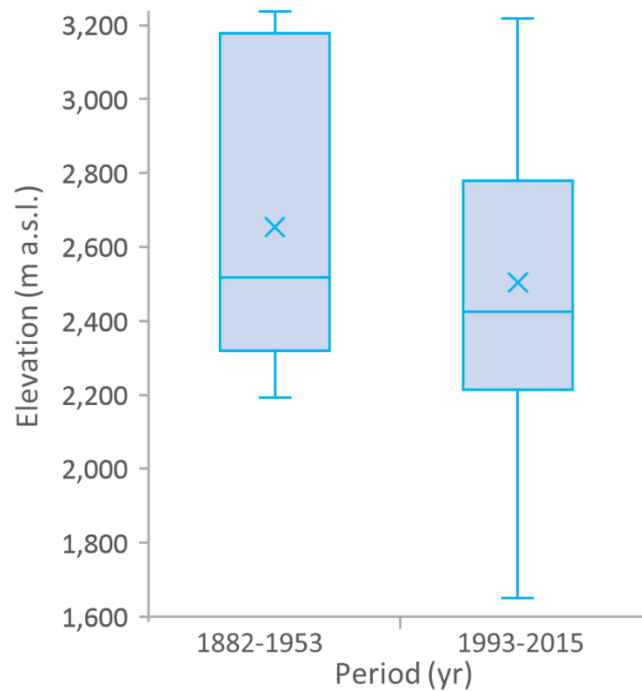
535

Figure 9: Boxplots for the elevations of the main deposits of snowfall-driven G-CHs during the periods 1882-1953 and 1993-2015.

23